

pulses radiated per antenna, and the number of antennas in an array. For example, if each pulse carries 1 mJ of energy, it would be permissible to couple up to 28,000 pulses into the breast over a 6 min period. In a practical UWB microwave radar imaging scenario, an array of antennas surrounds the breast volume and each element sequentially illuminates the breast. A typical array may contain on the order of 50 antennas, suggesting that up to 560 pulses could be transmitted by each antenna without exceeding the peak 1-g SA limit suggested in the IEEE exposure guideline. Note that the level of exposure of 560 pulses per antenna is much higher than we anticipate needing for this application.

#### 4. CONCLUSIONS

We have investigated the absorption of short (120 ps, 6-GHz-carrier) microwave pulses in anatomically realistic numerical breast phantoms in an effort to formally evaluate the safety of UWB microwave breast cancer detection technology operating in the 1–11 GHz range. We have found that the SA does not vary greatly with patient-to-patient variations in breast shape, tissue composition, or fibroglandular dielectric properties. While the specific characteristics (antenna radiation patterns, coupling media properties, etc.) of future clinical systems may differ from those assumed for this computational study, the SA values are not expected to vary significantly as a function of those characteristics. The normalized SA values reported in this paper can be scaled to account for the total number of pulses radiated and different pulse energies, providing valuable guidance in the design of future clinical systems that are in compliance with safety standards. For anticipated embodiments of such a system, we conclude that UWB microwave breast cancer detection modalities pose no health risk to the patient.

#### ACKNOWLEDGMENTS

This work was supported by the National Institutes of Health under grant F31 CA110942 awarded by the National Cancer Institute and the National Science Foundation under grant BES 0201880.

#### REFERENCES

1. S.C. Hagness, A. Taflove, and J.E. Bridges, Two-dimensional FDTD analysis of a pulsed microwave confocal system for breast cancer detection: Fixed-focus and antenna-array sensors, *IEEE Trans Biomed Eng* (1998), 1470–1478.
2. E.C. Fear and M.A. Stuchly, Microwave system for breast tumor detection, *IEEE Microwave Guided Wave Lett* 9 (1999), 470–472.
3. E.J. Bond, X. Li, S.C. Hagness, and B.D. Van Veen, Microwave imaging via space-time beamforming for early detection of breast cancer, *IEEE Trans Antennas Propag* (2003), 1690–1705.
4. X. Li, S.K. Davis, S.C. Hagness, D.W. van der Weide, and B.D. Van Veen, Microwave imaging via space-time beamforming: Experimental investigation of tumor detection in multilayer breast phantoms, *IEEE Trans Microwave Theory Tech* (2004), 1856–1865.
5. J.M. Sill and E.C. Fear, Tissue sensing adaptive radar for breast cancer detection—Experimental investigation of simple tumor models, *IEEE Trans Microwave Theory Tech* 53 (2005), 3312–3319.
6. A. Taflove and S.C. Hagness, *Computational electrodynamics: The finite-difference time-domain method*, 3rd ed., Artech House, Norwood, MA, 2005.
7. E. Zastrow, S.K. Davis, and S.C. Hagness, Safety assessment of breast cancer detection via ultrawideband microwave radar operating in swept frequency mode, In *Proceedings of IEEE International Symposium on Antennas and Propagation*, Albuquerque, NM, July 2006, in press.
8. X. Li, S.C. Hagness, M.K. Choi, and D.W. van der Weide, Numerical and experimental investigation of an ultrawideband ridged pyramidal horn antenna with curved launching plane for pulse radiation, *IEEE Antennas Wireless Propag Lett* (2003), 259–262.
9. M. Converse, E.J. Bond, B.D. Van Veen, and S.C. Hagness, A computational study of ultrawideband versus narrowband microwave hyperthermia for breast cancer treatment, *IEEE Trans Microwave Theory Tech* 54 (2006), 2169–2180.
10. W.T. Joines, Y. Zhang, C. Li, and R. L. Jirtle, The measured electrical properties of normal and malignant human tissues from 50 to 900 MHz, *Med Phys* (1994), 547–550.
11. A.J. Surowiec, S.S. Stuchly, J.R. Barr, and A. Swarup, Dielectric properties of breast carcinoma and the surrounding tissues, *IEEE Trans Biomed Eng* 35 (1988), 257–263.
12. S. Chaudhary, R. Mishra, A. Swarup, and J. Thomas, Dielectric properties of normal and malignant human breast tissue at radiowave and microwave frequencies, *Ind J Biochem Biophys* 21 (1984), 76–79.
13. S. Gabriel, R.W. Lau, and C. Gabriel, The dielectric properties of biological tissues. III. Parametric models for the dielectric spectrum of tissues, *Phys Med Biol* 41 (1996), 2271–2293.
14. J. Hilland, Simple sensor system for measuring the dielectric properties of saline solutions, *Meas Sci Technol* (1997), 901–910.
15. D.M. Lanners, K.K. Amrami, R.S. Jonsgaard, J.J. Gisvold, and J.P. Felmlee, Safety and MRI artifact evaluation at 1.5 T of metallic mounting sheath of a marking clip inadvertently deployed at stereotactic biopsy, *Am J Roentgenol* (2004), 825–829.
16. K. Caputa, M. Okoniewski, and M.A. Stuchly, An algorithm for computations of the power deposition in human tissue, *IEEE Antennas Propag Mag* 41 (1999), 102–107.
17. IEEE Standard for safety levels with respect to human exposure to radio frequency electromagnetic fields, 3 kHz to 300 GHz, IEEE Standard C95.1, 1999.

© 2006 Wiley Periodicals, Inc.

## APPLICATION OF THE FOLDY-LAX MULTIPLE SCATTERING METHOD TO THE ANALYSIS OF VIAS IN BALL GRID ARRAYS AND INTERIOR LAYERS OF PRINTED CIRCUIT BOARDS

C.-J. Ong,<sup>1</sup> D. Miller,<sup>2</sup> L. Tsang,<sup>1</sup> B. Wu,<sup>1</sup> and C.-C. Huang<sup>2</sup>

<sup>1</sup> Department of Electrical Engineering  
University of Washington  
Paul Allen Center, Room AE100R  
Campus Box 352500  
Seattle, WA 98195-2500

<sup>2</sup> Intel Corporation  
Jones Farm 5, 2111 N.E., 25th Avenue  
Hillsboro, OR 97124-5961

Received 12 May 2006

**ABSTRACT:** *The authors applied the method of Foldy-Lax multiple scattering equations to multiple vias in ball grid arrays and the interior layers of printed circuit boards. The method gives the scattering parameters of the array. The results are verified with Ansoft's HFSS with very little difference between the Foldy-Lax approach and the HFSS results. The CPU required for the method is only a small fraction of the time that HFSS requires. For a 16 × 16 array of vias, the method calculates all the S-parameters of the 512 ports in 4 min for 10 frequencies on a Pentium 3.2 GHz PC. © 2006 Wiley Periodicals, Inc. *Microwave Opt Technol Lett* 49: 225–231, 2007; Published online in Wiley InterScience (www.interscience.wiley.com). DOI 10.1002/mop.22091*

**Key words:** vias; multiple scattering; signal integrity; ball grid arrays; printed circuit boards

## 1. INTRODUCTION

Signal integrity engineers have to analyze the losses and crosstalk of vias in parallel plate structures in ball-grid arrays and the interior layers of printed circuit boards. Common full wave electromagnetic (EM) solvers used include Ansoft's HFSS based on the finite element method (FEM) and CST Microwave Studio based on the finite difference time domain (FDTD) method.

Besides FEM and FDTD, via structures have been analyzed using quasi-static approaches to extract the inductances and capacitances [1]. However at higher frequencies, full wave approaches are necessary to model the complex interactions between vias and the ground planes. Chen et al. have combined circuit models with 2D FDTD [2]. Gu et al. [3] and Hsu and Wu [4] have derived analytical approaches for a single via and applied it to multilayer stackups.

Recently, the Foldy-Lax multiple scattering method has been applied to the solution of scattering parameters of many vias in parallel plate structures [5, 6]. The method uses the antipads as the radiation sources and the vias are viewed as perfect electric conducting (PEC) scatterers. The method is 3D and includes full waveguide modes that have variation in  $\rho$ ,  $\phi$ , and  $z$ . A summation is done for the parallel plate waveguide modes  $l$  and the azimuthal variation orders  $n$ . For the near field interaction of densely packed vias, more waveguide modes and azimuthal variation orders are taken to achieve accurate results. The method is applicable even for cases where the vias are short and of large diameter if the number of modes and azimuthal variation orders are sufficient. The Foldy-Lax method is numerically efficient for the multiple via problem. (1) The method consists of analytic closed form expressions. (2) Only a few waveguide modes and azimuthal variation orders are required in near-field interactions. (3) Only one waveguide mode and azimuthal variation order is required in far-field interactions. (4) Only a few unknowns are required per via. The method has also been accelerated for analyzing a large number of vias using the preconditioned SMCG method [7].

In this article, we study complicated ball grid arrays (BGA) geometries with large number of vias and stacked up via arrays with the Foldy-Lax multiple scattering method. BGAs are commonly found IC surface-mount packages. Stacked-up via arrays are commonly found on multilayer printed circuit boards. Numerical results are illustrated as a function of frequency and for the scattering matrices of multiple ports. The results are verified with Ansoft's HFSS with very little difference between the Foldy-Lax approach and the HFSS results. The CPU and memory requirement are compared with HFSS and are shown to be much less.

## 2. FOLDY-LAX MULTIPLE SCATTERING METHOD FOR MULTIPLE-LAYERS OF VIAS

For a printed circuit board, there are the exterior and interior layers. The whole problem can be decomposed into an exterior and

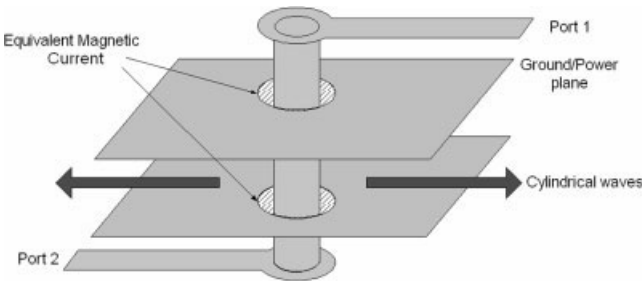


**Figure 1** Equivalent magnetic current on antipad between exterior and interior problems

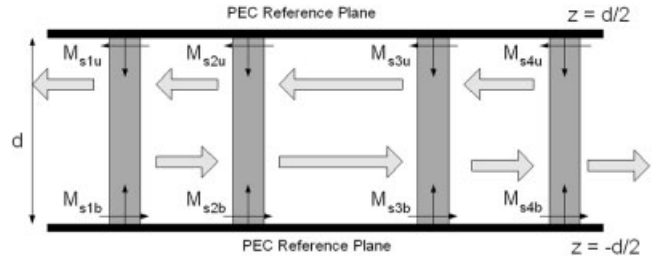


**Figure 2** Multiple vias in the interior problem

interior problem by introducing equivalent magnetic frill currents on the antipads. Figure 1 shows the equivalent magnetic current on the antipad for a via. The two problems can be solved separately and combined by equating the current on the via and the voltage on the antipad.

Figure 2 show multiple cylinders in an interior problem. The Foldy-Lax multiple scattering equations [5, 6] are as follows.

The final exciting magnetic field on cylinder  $p$  is

$$\bar{H}_{ex}^{(p)} = \sum_{m,l} w_{lm}^{TM(p)} Rg \bar{H}_m^{TM}(k_{pl}, k_{z,l}, \bar{\rho} - \bar{\rho}_p, z \pm d/2)$$

where  $w_{lm}^{TM(p)}$  is the final exciting field coefficients to be solved,  $l$  is the parallel plate waveguide mode,  $\bar{\rho}_p$  is the position vector of the center of via  $p$  in the  $x$ - $y$  plane and  $Rg \bar{H}_m^{TM}$  is the magnetic TM modal solution given by

$$Rg \bar{H}_n^{TM}(k_{\rho}, k_z, \bar{\rho}, z) = \frac{j}{\eta} \left[ -\hat{\rho} \frac{jn}{\rho} J_n(k_{\rho}\rho) - \hat{\phi} k_{\rho} J_n'(k_{\rho}\rho) \right] e^{-jn\phi} \cos(k_z z)$$

$n$  is the azimuthal variation order.

The Foldy-Lax multiple scattering equation governs the final exciting field coefficient:

$$w_{ln}^{TM(q)} = a_{ln}^{TM(q)} + \sum_{\substack{p=1 \\ p \neq q}}^N \sum_{m=-\infty}^{\infty} H_{n-m}^{(2)}(k_{\rho l} |\bar{\rho}_p - \bar{\rho}_q|) e^{j(n-m)\phi_{\bar{\rho}_p, \bar{\rho}_q}} T_m^{(N)} w_{lm}^{TM(p)}$$

where  $T_m^{(N)}$  is the T-matrix coefficient for PEC cylinders given by

$$T_m^{(N)} = -\frac{J_m(k_{\rho l} a)}{H_m^{(2)}(k_{\rho l} a)}$$

where  $a$  is the radius of the via.  $a_{ln}^{TM(q)}$  are the incident field coefficients from the magnetic current sources from either the upper or lower reference planes.

To calculate that we consider the magnetic frill current at aperture  $i$  with  $M_{su}$  at  $z' = d/2$  given by

$$\bar{M}_{su}(\bar{\rho}') = -\frac{V_{iu}}{|\bar{\rho}' - \bar{\rho}_i| \ln(b/a)} \hat{\phi}_{pp}, \text{ for } a \leq |\bar{\rho}' - \bar{\rho}_i| \leq b$$

where  $b$  is the radius of the antipad and  $V_{iu}$  is the voltage of the upper antipad of via  $i$ . The expression for the magnetic current at the bottom plane  $M_{sb}$  at  $z' = -d/2$  has  $V_{ib}$  instead of  $V_{iu}$ .

For all the magnetic current sources at the upper plane ( $z' = d/2$ ), the incident wave at cylinder  $q$  is

$$a_{\text{in}}^{TM(q)} = \frac{jk}{2d} \frac{(-1)^{n+1}}{k_{\rho l}^2} f_l \frac{2\pi}{\ln(b/a)} (V_{qu} \delta_{n0} [H_0^{(2)}(k_{\rho l} b) - H_0^{(2)}(k_{\rho l} a)] + \sum_{i \neq q}^N H_n^{(2)}(k_{\rho l} |\bar{\rho}_q - \bar{\rho}_i|) e^{jn\phi_{\bar{\rho}_q \bar{\rho}_i}} \{V_{iu} [J_0(k_{\rho l} b) - J_0(k_{\rho l} a)]\})$$

$f_l$  is 0.5 if  $l = 0$  and 1 otherwise.  $\delta_{n0}$  is 1 for  $n = 0$  and 0 otherwise. The incident wave due to the magnetic current sources at the lower plane are found by replacing  $V_{qu}$  and  $V_{iu}$  by  $V_{qb}$  and  $V_{ib}$  respectively in the above expression

We can thus solve for  $w_{\text{in}}^{TM(q)}$  and get the current on cylinder  $p$ , which is given by

$$I^{(p)} = 2\pi a \sum_l w_{l0}^{TM(p)} k_{\rho l} \frac{2}{\pi k_{\rho l} a H_0^{(2)}(k_{\rho l} a) \eta} \cos[k_{z l} (z \pm d/2)]$$

We can thus solve for all the currents at the antipads due to the sources at the upper and lower antipads. We can get a resulting admittance matrix for the interior problem, which can be converted to a scattering matrix.

Note that in the Foldy–Lax equations, there is a double summation over the waveguide modes and over the azimuthal variation orders,

$$l = 0, 1, 2, \dots, \infty.$$

$$n = -\infty, \dots, \infty.$$

however, in practice only a small finite number of summations are needed as follows:

$$l = 0, 1, 2, \dots, l_{\text{max}}$$

$$n = -N_{\text{max}}, \dots, N_{\text{max}}$$

### 2.1. Choice of Number of Modes $l_{\text{max}}$ and the Number of Harmonics $N_{\text{max}}$

For the far-field where  $\rho > \lambda$ , we only need the lowest order modes for the waveguide and the azimuthal variation orders. For the near-field where  $\rho < \lambda$ , for the maximum number of azimuthal variation orders, we can choose:

$$N_{\text{max}} = \text{floor}(2ka) + 1$$

The floor function gives the integer value closest to and lower than the argument. For the maximum number of waveguide modes in the near field, we note that

$$k_{\rho l} = \sqrt{k^2 - k_{z l}^2}$$

if  $k_{z l} > k$  and  $k_{\rho l} \rho$  is large, the evanescent field decays as  $\exp(-k_{\rho l} \rho)$ . We can let  $\max(k_{\rho l}) = 5/\rho$ . Then

$$l_{\text{max}} = \text{floor} \left[ \frac{d}{\pi} \sqrt{\left( \frac{5}{\rho} \right)^2 - k^2} \right]$$

next we extend the formalism to include multiple vias in multiple layered structures.

Figure 3 shows the equivalent network for an N-via interior problem. The currents and voltages in the diagram are all  $N \times 1$  column vectors. The network parameters we obtain from the

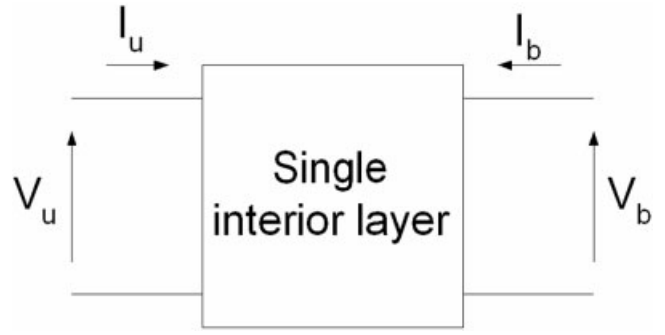


**Figure 3** Equivalent network for N via (port) single layer interior problem

Foldy–Lax method are for the admittance matrix. The matrix equation is

$$\begin{bmatrix} I_u \\ I_b \end{bmatrix} = \begin{bmatrix} Y_{uu} & Y_{ub} \\ Y_{bu} & Y_{bb} \end{bmatrix} \begin{bmatrix} V_u \\ V_b \end{bmatrix}$$

Each  $Y$  submatrix is of dimension  $N \times N$ . To cascade the interior problems, we transform the admittance matrix to the transmission ( $ABCD$ ) matrix.

$$\begin{bmatrix} V_u \\ I_u \end{bmatrix} = \begin{bmatrix} A & B \\ C & D \end{bmatrix} \begin{bmatrix} V_b \\ -I_b \end{bmatrix}$$

The transformation equations can be derived to be as follows:

$$A = -Y_{bu}^{-1} Y_{bb}$$

$$B = -Y_{bu}^{-1}$$

$$C = -Y_{uu} Y_{bu}^{-1} Y_{bb} + Y_{ub}$$

$$D = -Y_{uu} Y_{bu}^{-1}$$

After multiplying the transmission matrices for each layer to get the cascaded transmission matrix, it can be converted back to the admittance matrix as follows:

$$Y_{uu} = DB^{-1}$$

$$Y_{ub} = C - DB^{-1}A$$

$$Y_{bu} = -B^{-1}$$

$$Y_{bb} = B^{-1}A$$

The admittance matrix can be converted to the scattering matrix by the following equation:

$$S = (Y_0 U + Y)^{-1} (Y_0 U - Y)$$

where  $U$  is the identity matrix and  $Y_0$  is the characteristic admittance of the coaxial port formed by the antipad and the via.

$$Y_0 = \frac{2\pi}{\eta \ln(b/a)}$$

To analyse cases where there are ground vias and signal vias, the  $Y$  matrix corresponding to the signal vias is extracted from the entire  $Y$  matrix of ground and signal vias.

**TABLE 1 Run Time Per Frequency for the Various Via Array Sizes on Ansoft HFSS and the Foldy–Lax Approach**

Size of via array	Run Time Per Frequency on Intel Pentium 3.2-GHz PC With 4 GB of RAM	
	Ansoft HFSS	Foldy–Lax Approach
$2 \times 2$	17 s	0.14 s
$4 \times 4$	2 min 42 s	0.25 s
$8 \times 8$	Approx. 1 hr	1.47 s
$16 \times 16$	Insufficient memory	24 s

### 3. NUMERICAL RESULTS AND DISCUSSION

In this section, we use the Foldy–Lax approach to study signal integrity problems of complicated BGA geometries with large number of vias and stacked-up via arrays with the Foldy–Lax multiple scattering method. We discuss the physics of the numerical results as a function of frequency and for the scattering matrices of multiple ports.

#### 3.1. CPU Comparison Between HFSS and Foldy–Lax Approach

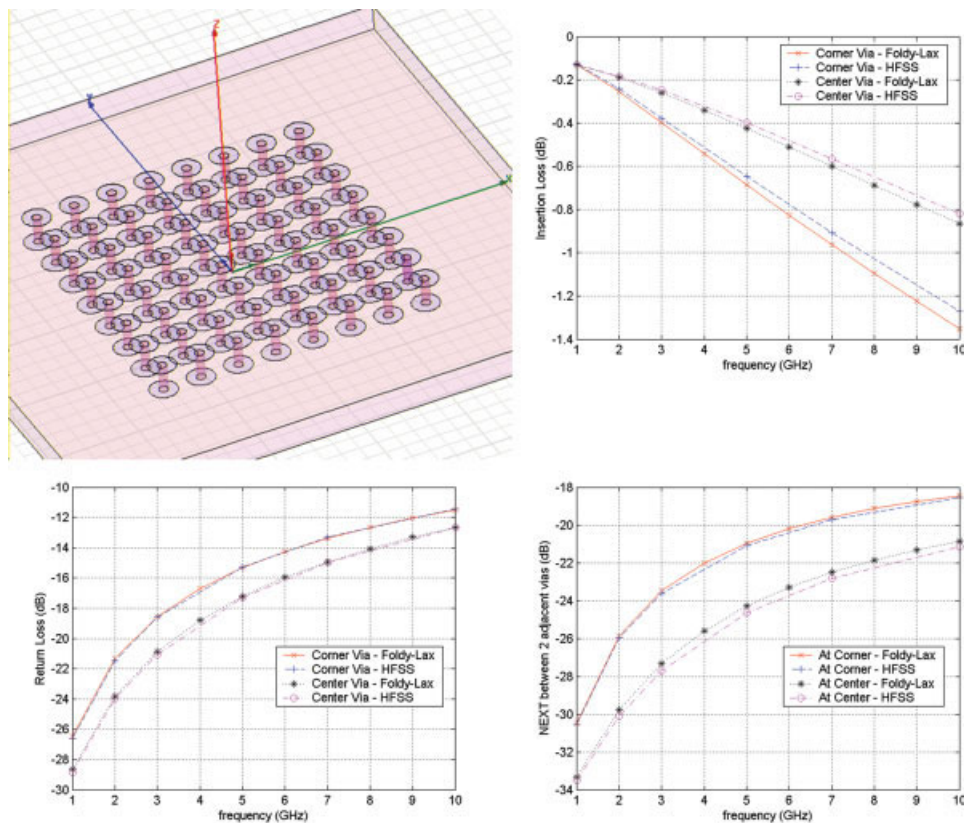
Table 1 shows the run time per frequency for various via array sizes on both Ansoft HFSS and the Foldy–Lax approach. It can be seen that the Foldy–Lax approach is able to simulate the S-parameters of via arrays in a small fraction of the time that HFSS takes. The Foldy–Lax approach can even solve  $16 \times 16$  arrays, which HFSS cannot solve on a PC with 4 GB of RAM due to memory problems.

#### 3.2. Results $8 \times 8$ via Array

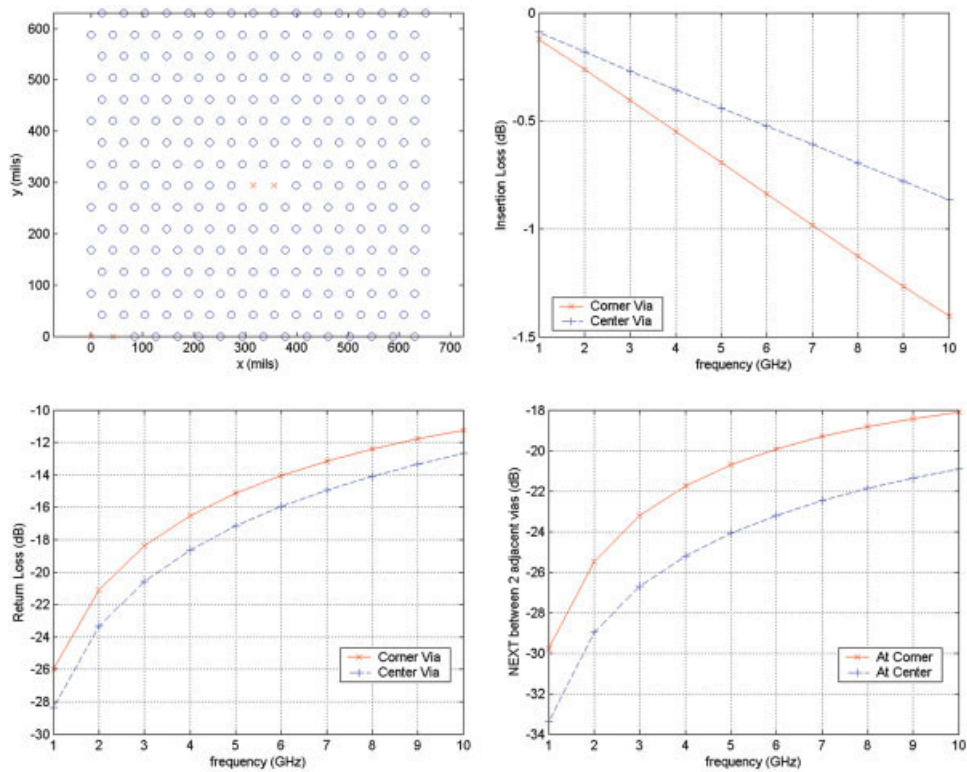
Figure 4(a) shows an  $8 \times 8$  via array. The via radius  $a$  is 5 mils and the antipad radius  $b$  is 15 mils. The distance between the reference planes  $d$  is 30 mils. The vias are spaced by 42 mils in both the  $x$  and  $y$  directions. The dielectric constant  $\epsilon_r$  is 4.

Figure 4(b) shows the insertion losses for both a via at a corner of the  $8 \times 8$  array and a via at the center of the array. There is greater loss in general at high frequencies mainly because of radiation losses rather than conductor losses, since the via and the ground planes are modeled as PECs. It can be seen that the results between the Foldy–Lax method and HFSS differ by at most 0.1 dB at 10 GHz for the corner via. The via at the center show less insertion loss than the via at the corner of the array. The reason is that the signal traveling on the via at the corner will see a greater change in characteristic impedance as the reference plane gets further as the signal goes down the via. Vias surrounding the signal via reduce the change in the impedance. The center via has more neighbouring vias than the corner via and hence will have a smaller change in impedance along the via. Also, the via at the corner has more power being radiated away whereas the via at the center is shielded by vias all around.

Figure 4(c) shows the return losses for the via at a corner of the  $8 \times 8$  array and the via at the center of the array. The agreement between the HFSS and the Foldy–Lax results are excellent. There is more reflection for the corner via compared to that of the center via. This is also due to the greater change in impedance for the corner via. Another possible reason for the reduced reflection for the center via is because more power is being coupled to the other vias.



**Figure 4** (a) (above left)  $8 \times 8$  via array, (b) (above right) insertion losses, and (c) (below left) return losses of corner via and center via (Foldy–Lax and HFSS). (d) (below right) Near-end crosstalk (NEXT) of corner via and adjacent via and NEXT of two center vias (Foldy–Lax and HFSS). [Color figure can be viewed in the online issue, which is available at [www.interscience.wiley.com](http://www.interscience.wiley.com)]



**Figure 5** (a) (above left) Schematic diagram of  $16 \times 16$  array with alternate row offset. The o's mark the position of the vias. The x's mark the position of the corner vias and the center vias being considered. The insertion loss and return loss are taken for the left via in each pair. (b) (above right) Insertion losses and (c) (below left) return losses of corner via and center via (Foldy-Lax). (d) (below right) NEXT of corner via and adjacent via and NEXT of two center vias (Foldy-Lax). [Color figure can be viewed in the online issue, which is available at [www.interscience.wiley.com](http://www.interscience.wiley.com)]

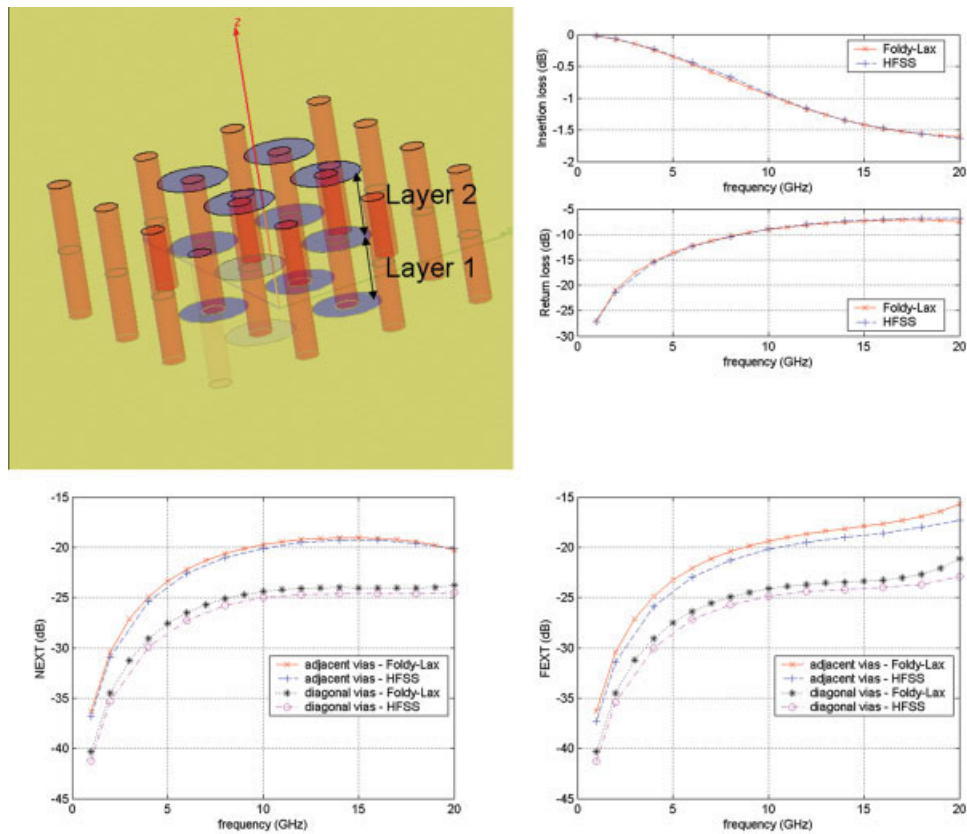


**Figure 6** (a) (above left) Vias in a two layer stack up.  $4 \times 4$  array with a  $2 \times 2$  array of signal vias in the center. The rest are ground vias. (b) (above right) Insertion loss and return loss for a signal via (Foldy-Lax and HFSS). (c) (below left) NEXT between adjacent vias and diagonal vias (Foldy-Lax and HFSS). (d) (below right) FEXT between adjacent vias and diagonal vias (Foldy-Lax and HFSS). [Color figure can be viewed in the online issue, which is available at [www.interscience.wiley.com](http://www.interscience.wiley.com)]

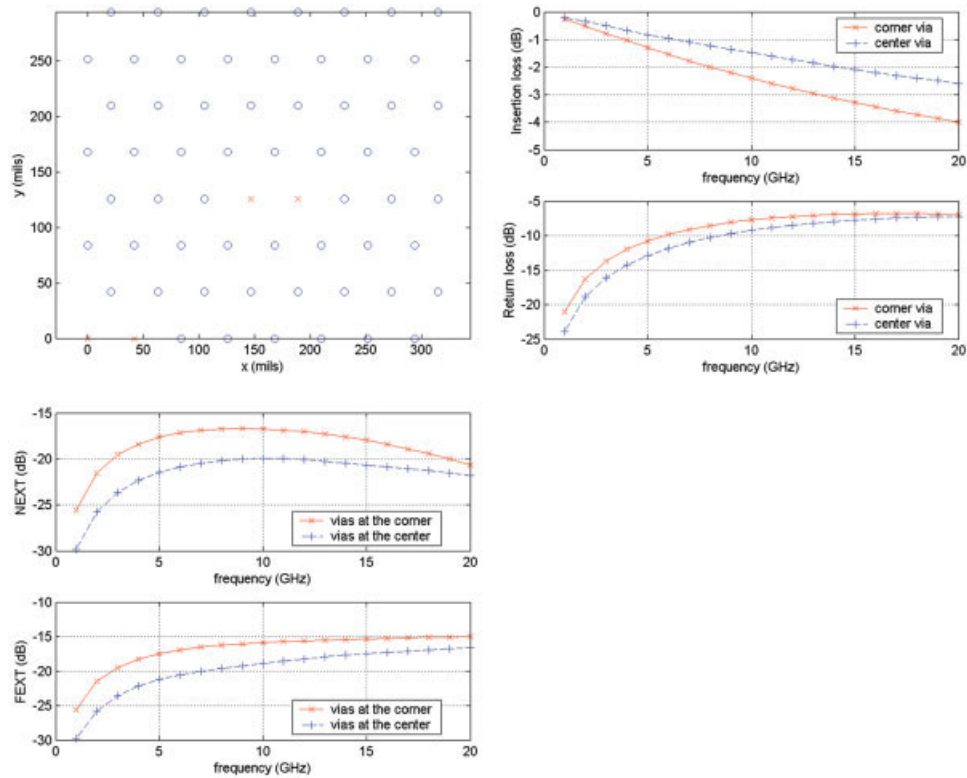


**Figure 7** (a) (above left) Schematic diagram of an  $8 \times 8$  two-layer stacked array with alternate row offset. The o's mark the position of the vias. The x's mark the position of the corner vias and the center vias being considered. The insertion loss and return loss are taken for the left via in each pair. (b) (above right) Insertion loss and return loss for corner and center via (Foldy-Lax). (c) (below left) NEXT and FEXT for vias at the corner and also for vias at the center (Foldy-Lax). [Color figure can be viewed in the online issue, which is available at [www.interscience.wiley.com](http://www.interscience.wiley.com)]

Figure 4(d) shows the near end crosstalk (NEXT) between two adjacent vias at a corner and the NEXT between two adjacent vias at the center of the  $8 \times 8$  array. The difference between the HFSS and Foldy-Lax results for the vias at the center is at most 0.5 dB. Vias generally have greater coupling at higher frequencies. This is because the mutual impedance increases with frequency if the mutual inductance does not change much. The vias at the corner have more crosstalk than the vias at the center. This is because the vias at the corner have less neighboring vias to couple power to. The vias at the center couple less power to each neighboring via than the corner via.

### 3.3. Results of $16 \times 16$ Array

Figure 5(a) shows a schematic diagram of the positions of the vias for a  $16 \times 16$  array with alternate rows offset by 21 mils. The rest of the physical parameters are the same as the  $8 \times 8$  array. The x's mark the position of the corner and center vias being considered for the NEXT. The insertion losses and return losses are taken for the left via in each pair.

Figures 5(b) and 5(c) show the insertion losses and the return losses respectively of the corner and center via in the  $16 \times 16$  array. The insertion loss for the center via is again less than that of the corner via. There is more reflection from the corner via

**TABLE 2 Comparison of HFSS and Foldy-Lax Results for the  $8 \times 8$  Via Array in a 2-Layer Stackup With Alternate Rows Offset by 21 mils**

	Freq. (GHz)	Corner Via			Center Via		
		Foldy-Lax result (dB)	HFSS result (dB)	Diff. (dB)	Foldy-Lax result (dB)	HFSS result (dB)	Diff. (dB)
Insertion loss	1	-0.248636	-0.223837	0.024799	-0.202639	-0.19616	0.006479
	5	-1.290846	-1.235191	0.055655	-0.819758	-0.786663	0.033095
	10	-2.408438	-2.328585	0.079853	-1.481284	-1.439423	0.041861
Return loss	1	-21.09212	-22.8565	1.764377	-23.90615	-24.07405	0.167903
	5	-10.75235	-10.76883	0.01648	-12.89517	-12.80335	0.091825
	10	-7.732318	-7.590406	0.141912	-9.212929	-9.054727	0.158202
NEXT	1	-25.58751	-26.29301	0.705504	-29.81221	-30.16216	0.349954
	5	-17.64353	-17.71082	0.067293	-21.47859	-21.71319	0.234608
	10	-16.7601	-16.7393	0.020796	-19.95081	-20.11427	0.163461
FEXT	1	-25.58161	-26.38898	0.807378	-29.8027	-30.3139	0.511204
	5	-17.4823	-17.67695	0.194648	-21.23637	-21.71369	0.477323
	10	-15.86297	-15.99048	0.127505	-18.89247	-19.38547	0.493005

compared to that of the center via. The reasons are similar to that of the  $8 \times 8$  array. Figure 5(d) shows the NEXT between the pair of vias at the corner and the NEXT between the pair of vias at the center. The crosstalk of the corner vias is again greater than that of the center via. It is interesting to see that the crosstalk of the adjacent vias in the corner of the offset array is slightly greater than that of the regular array. This is because the vias between rows in the offset array are further apart and hence less energy is coupled to the other rows.

Figure 6(a) shows a  $4 \times 4$  array in a two-layer stackup. The center  $2 \times 2$  array consist of signal vias. The rest of the vias are ground vias. The via and spacing parameters are the same as the  $8 \times 8$  array.

Figure 6(b) (top) shows the insertion loss of a signal via in the two layer stackup. The difference between the Foldy–Lax method and the HFSS result is less than 0.05 dB. Figure 6(b) (bottom) shows the return loss of a signal via. The agreement between the tool and HFSS is very good. It is interesting to see that the insertion and return losses do not monotonically increase with frequency, but rather taper off at high frequencies near 20 GHz. In fact, the vias that are three spacings apart (126 mils) will resonate at about 23 GHz.

### 3.4. Results of $4 \times 4$ Array in a Two-Layer Stackup

Figure 6(c) shows the NEXT between adjacent signal vias and between the diagonal signal vias. The difference between the Foldy–Lax result and the HFSS result is within 1 dB. Figure 6(d) shows the far-end crosstalk (FEXT). The difference between the Foldy–Lax and HFSS results is about 2 dB at 20 GHz but is within 1 dB for most other frequencies. It can be seen that at higher frequencies, both the Foldy–Lax and HFSS show that the NEXT is different from the FEXT. A few observations about the results: The crosstalk for the diagonal vias is always lower than that of adjacent vias because the vias in the former case are further apart. The NEXT seems to taper off at about 12 GHz and remains quite constant over a range of frequencies. Maximum power is being transferred between the two near end ports at those frequencies. The FEXT is much the same as the NEXT except at very high frequencies. At high frequencies, the FEXT is greater than the NEXT. This is because the more power is being coupled along the length of the via at those high frequencies.

### 3.5. Results of $8 \times 8$ via Array in a Two-Layer Stackup

Figure 7(a) shows a schematic diagram of the positions of the vias in an  $8 \times 8$  via array in a two-layer stackup with alternate rows offset by 21 mils. The physical parameters are the same as the previous  $4 \times 4$  array, except that there are no ground vias. The o's mark the positions of the vias. The x's mark the position of the corner and center vias being considered in the next few figures. Insertion and return losses are taken on the left via of each pair.

Table 2 shows the comparison between the HFSS and the Foldy–Lax results for the  $8 \times 8$  array in the two-layer stackup. The HFSS simulations were run at 1, 5, and 10 GHz as the run times were between 1 and 2 h per frequency on a 3.2 GHz PC with 4 GB of RAM. It can be seen that the difference in the insertion losses is at most 0.08 dB at 10 GHz. The maximum difference in the return loss was nearly 2 dB for the corner via at 1 GHz. But the return loss is below  $-20$  dB at 1 GHz, so the difference is not that significant. Other frequencies for the corner via and all the other frequencies for the center via gives much better comparisons of the return loss. The difference in NEXT and FEXT results were all below 1 dB for all frequencies.

Figure 7(b) (top) shows the insertion losses of the corner and center via in the  $8 \times 8$  array in the two-layer stackup. As usual, the center via will have less insertion losses than the corner via for reasons mentioned previously. Figure 7(b) (bottom) shows the returns losses

for the same corner and center via. The corner via has greater return loss. The corner via has almost the same return loss as the center via near 20 GHz. At that frequency, the impedance seen by the port must be similar for both vias. Figure 7(c) (top) shows the NEXT between the corner vias and the NEXT between the center vias in the  $8 \times 8$  array in the two-layer stackup. The NEXT actually decreases with frequency above 10 GHz resulting in a maximum NEXT at that point. Closer examination will reveal that vias seven spacings apart (294 mils) will resonate at 10 GHz. This explains the maximum NEXT for the center via at that frequency. Figure 7(c) (bottom) shows the corresponding FEXT between the corner vias and the FEXT between the center vias.

## ACKNOWLEDGMENT

The research in this article was supported by a research grant from INTEL to the University of Washington.

## REFERENCES

- Q. Li, L. Tsang, and H. Chen, Quasi-static parameters, low-frequency solutions, and full-wave solutions of a single-layered via, *Microwave Opt Technol Lett* 35 (2002), 34–40.
- Y. Chen, Z. Wu, A. Agrawal, Y. Liu, and J. Fang, Modeling of  $\delta$ -I noise in digital electronics packaging, in proceedings of the IEEE multi-chip module conference, MCMC'94, Santa Cruz, CA, March 15–17, 1994, pp. 126–131.
- Q. Gu, Y.E. Yang, and M. Ali, Modeling and analysis of vias in multilayered integrated circuits, *IEEE Trans Microwave Theory Tech* 41 (1993), 206–214.
- S.-G. Hsu and R.-B. Wu, Full-wave characterization of a through hole via in multilayered packaging, *IEEE Trans Microwave Theory Tech* 43 (1995), 1073–1081.
- L. Tsang, H. Chen, C.-C. Huang, and V. Jandhyala, Modeling of multiple scattering among vias in planar waveguides using Foldy–Lax equations, *Microwave Opt Technol Lett* 31 (2001), 201–208.
- L. Tsang, J.A. Kong, K.-H. Ding, and C.O. Ao, Multiple scattering by cylinders in the presence of boundaries, *Scattering of electromagnetic waves: Numerical simulations*, Wiley, New York, 2001, Ch. 12.
- C.-C. Huang, L. Tsang, C.H. Chan, and K.-H. Ding, Multiple scattering among vias in planar waveguides using preconditioned SMCG method, *IEEE Trans Microwave Theory Tech* 52 (2004), 20–28.

© 2006 Wiley Periodicals, Inc.

## ACCURATE EQUIVALENT CIRCUIT FOR ETCHED RESONATOR WITH EFFECTIVE NEGATIVE PERMITTIVITY

Hung-Wei Wu,<sup>1</sup> Min-Hang Weng,<sup>2</sup> Yan-Kuin Su,<sup>1</sup> Ru-Yuan Yang,<sup>1</sup> and Cheng-Yuan Hung<sup>1</sup>

<sup>1</sup> Advanced Optoelectronic Technology Center  
Department of Electrical Engineering  
Institute of Microelectronics  
National Cheng Kung University, Taiwan  
<sup>2</sup> National Nano Device Laboratories  
Taiwan

Received 13 May 2006

**ABSTRACT:** This letter demonstrates an accurate equivalent circuit for a negative permittivity resonator using single-cell complementary split ring resonator underneath a microstrip line that introduces two attenuation poles in desired frequencies. The proposed equivalent circuit consists of lumped elements that can be accurately extracted from the measured S-parameters. Good agreement with response of equivalent circuit, electromagnetic simulation, and measurement is demon-